# Ultrafast Nonlinear Optical Response of a Single Gold Nanorod near Its Surface Plasmon Resonance

H. Baida,[1] D. Mongin,[1] D. Christofilos,[1,2] G. Bachelier,[1] A. Crut,[1] P. Maioli,[1] N. Del Fatti,[1,*] and F. Vallée[1]

[1]*Université Lyon 1, CNRS, LASIM, 43 Boulevard du 11 Novembre, 69622 Villeurbanne cedex, France*

[2]*Physics Division, School of Technology, Aristotle University of Thessaloniki, 54124 Thessaloniki, Greece*

(Received 13 May 2011; published 28 July 2011)

The ultrafast optical nonlinearity of an optically characterized single gold nanorod is investigated around its surface plasmon resonance, by combining a far-field spatial modulation technique with a high sensitivity pump-probe setup. The spectrally and temporally dependent response is quantitatively interpreted in terms of the bulklike optical nonlinearity enhanced by the plasmonic effect. The plasmon resonance dynamics is shown to be mostly governed by nonequilibrium electron and phonon processes. Their contributions to the nonlinear optical response of a single metal nano-object are elucidated, and the latter is connected to the nonlinearities of ensembles.

DOI: 10.1103/PhysRevLett.107.057402 PACS numbers: 78.67.Qa, 78.40.Kc, 78.47.J−, 78.67.Bf

Plasmonic effects are the key features dominating the linear and nonlinear optical responses of confined metallic systems [1–3]. These show up by localized or propagating surface plasmon resonances (SPR) depending on the system dimensionality, e.g., in metal nanoparticles or in nanowires and interfaces. The resonance amplitude and its spectral characteristics are very sensitive to the system properties and to its environment. It has been exploited in optical detection or in light manipulation at a subwavelength scale [4–7]. It also offers a large potential for ultrafast manipulation of the optical response and active control of light propagation using the metal optical nonlinearity [8]. However, its full exploitation requires detailed understanding and modeling of the nonlinear optical response of metallic systems at nanoscale.

The optical nonlinearity in bulk metals has been extensively investigated by using time-resolved femtosecond spectroscopy [9]. In nanosystems, though many results have been obtained on ensemble of nano-objects [2,10], quantitative comparison with theoretical models and investigation of plasmonic effects are hampered by the geometry, orientation, and environment distributions of the particles. As for the linear response [11–13], this averaging can be avoided by investigating a single nanoparticle. However, this approach has been scarcely used up to now and in single wavelength experiments [14,15], yielding only partial results and precluding their precise modeling. In this work we have investigated the spectral- and time-dependent response of a model system: single gold nanorods, which exhibit spectrally isolated SPR [16–18]. The nanorod is first optically detected and characterized *in situ* via measurement of its linear spectrum by spatial modulation spectroscopy (SMS) [19]. Its nonlinear optical response is subsequently measured around its SPR by using a two-color femtosecond pump-probe technique. Comparison with a theoretical model shows that the plasmon resonance dynamics reflects electron and lattice nonequilibrium effects and permits one to disentangle their contributions to the plasmonic optical nonlinearity.

Briefly, the SMS technique is based on modulation of the position of a nano-object in the focal spot of a tightly focused light beam [19]. In the presence of an absorbing and/or scattering nanoparticle, modulation of the transmitted power is induced. Its amplitude is proportional to the particle extinction cross section $\sigma_{\text{ext}}$, which can thus be quantitatively determined. By performing wavelength- and polarization-dependent measurements, an optical signature of the nano-object is obtained, which permits optical determination of its volume and shape [19,20] and, for a nanorod, its orientation [18]. The light source for the SMS setup uses the Ti:sapphire oscillator further used for time-resolved experiments. It delivers 150 fs pulses tunable in the 780–850 nm range, around the longitudinal SPR of the nanorods (Fig. 1). The pulse train is split into two parts, one providing the probe beam, the other being frequency-doubled to create the pump pulses (in the range 390–425 nm). SMS measurements were performed by using either these beams or part of a supercontinuum created in a photonic crystal fiber [19].

The samples were prepared from a colloidal solution of gold nanorods. Transmission electron microscopy (TEM) indicates cigarlike shapes that can be modeled as cylinders of width $W$ (in the range 8–13 nm), end-capped with hemispheres (Fig. 1). The extinction spectrum of the solution shows the longitudinal SPR of the nanorods around 780 nm (Fig. 1), consistent with their mean aspect ratio $\langle \eta \rangle = \langle L/W \rangle \approx 3.5$. The low surface density samples necessary for single particle optical studies were prepared by spin-coating the initial solution on a glass coverslip, after adding a polymer (polyvinyl alcohol, PVOH). Nanorods embedded in a thin polymer layer were obtained, providing them with a quasihomogeneous optical environment of dielectric constant $\epsilon_m$ [18,19].

 

As expected, the extinction cross-section spectrum of a single nanorod shows a narrow longitudinal SPR for light polarized along its main axis (Fig. 1). The nanorod aspect ratio $\eta$ and volume $V$ were determined by quantitatively reproducing its experimental $\sigma_{\text{ext}}$ spectrum by using finite element method simulations (assuming a cigarlike shape and $\epsilon_m = 2.1$) [18]. The bulk gold dielectric function was used with a weak electron-surface scattering correction [13,17,21]. As $\eta$ and $V$ reflect in different observables (the SPR wavelength $\lambda_R$ and the $\sigma_{\text{ext}}$ amplitude, respectively), they can be precisely determined. The accuracy of this optical characterization has been confirmed by performing TEM and optical measurements on the same nanorod, as previously done for metal nanospheres [20]. For the nanorod of Fig. 1, one thus obtains $\eta \approx 3.6$ and $V \approx 4400$ nm$^3$ (yielding $L = 43$ nm and $W = 12$ nm). In this size regime, $\sigma_{\text{ext}}$ is dominated by absorption, scattering contributing to about 4% of $\sigma_{\text{ext}}(\lambda_R)$.

Femtosecond pump-probe experiments are subsequently performed by focusing both the fundamental and frequency-doubled beams on the nanorod. The latter (pump beam) excites the electrons of the gold particle by interband absorption, and the former (probe beam) monitors the pump-induced change of the sample transmission, $\Delta T(\lambda_{\text{pr}}, t_D)$, as a function of the pump-probe time delay $t_D$. For a single nano-object located at the center of the probe beam focal spot, $\Delta T$ is proportional to modification of its extinction cross section: $\Delta T/T \approx -\Delta\sigma_{\text{ext}}(\lambda_{\text{pr}}, t_D)/S_{\text{pr}}$ (with $S_{\text{pr}} = \pi d_{\text{FWHM}}^2/(4\ln 2)$ for a Gaussian spot of full width at half maximum $d_{\text{FWHM}}$) [15]. In the weak excitation regime used here, the $\Delta T/T$ amplitude is proportional to the pump intensity, i.e., to the pump energy absorbed by the nanorod. This is precisely determined from SMS measurement of the absorption cross section at the pump wavelength, yielding for the nanorod of Fig. 1 $\sigma_{\text{abs}} \approx 200$ nm$^2$. As the nanoparticle volume $V$ is known, the absorbed energy density per pulse can be computed: $u_{\text{abs}} = \sigma_{\text{abs}} U_{pp}/S_{pp} V \approx 3 \times 10^6$ J/m$^3$ ($U_{pp} \approx 5$ fJ is the pump energy per pulse and $S_{pp}$ the pump focal spot area). By assuming instantaneous electron internal thermalization, this translates into an initial electron temperature rise $\Delta T_e^{\max} = \sqrt{T_0^2 + 2u_{\text{abs}}/c_0} - T_0 \approx 125$ K, characterizing the particle excitation ($T_0$ is the initial temperature and $c_0 T_0$ the initial electron heat capacity) [22].

The time dependence of $\Delta\sigma_{\text{ext}}(\lambda_{\text{pr}}, t_D)$ measured for the nanorod of Fig. 1 is shown in Fig. 2(a) for different probe wavelengths $\lambda_{\text{pr}}$ around its SPR. For $\lambda_{\text{pr}}$ larger or smaller than $\lambda_R$, an increase or decrease of $\Delta\sigma_{\text{ext}}$ is observed, respectively. For all $\lambda_{\text{pr}}$, $\Delta\sigma_{\text{ext}}(\lambda_{\text{pr}})$ subsequently decay with the same time constant $\tau_{e\text{-ph}}$ reflecting cooling of the excited electrons by energy transfer to the lattice ($\tau_{e\text{-ph}} \approx 1.1$ ps, consistent with the results in bulk gold and large gold nanoparticles for weak excitation [10]). When probing at the SPR wavelength $\lambda_{\text{pr}} \approx \lambda_R$, a transient reduction of $\Delta\sigma_{\text{ext}}$ is observed, followed by a slow rise of $|\Delta\sigma_{\text{ext}}|$ toward a constant value, with the time $\tau_{e\text{-ph}}$ [Fig. 2(a)]. The main temporal and spectral behaviors can be interpreted in terms of transient redshift and broadening of the SPR, as in an ensemble of gold nanorods [23] and

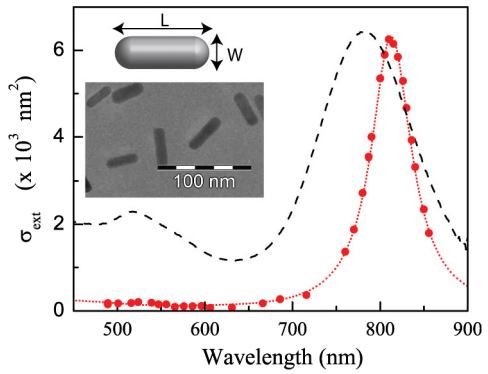


FIG. 1 (color online). TEM image and typical cigarlike shape of the gold nanorods. Dots: Absolute extinction cross-section spectrum of a single gold nanorod deposited on a glass substrate and embedded in PVOH, measured with SMS for light polarized along its long axis. Dotted line: Fit based on finite element method computations with $L = 43$ nm and $W = 12$ nm. Dashed line: Normalized ensemble spectrum of the original colloidal solution.

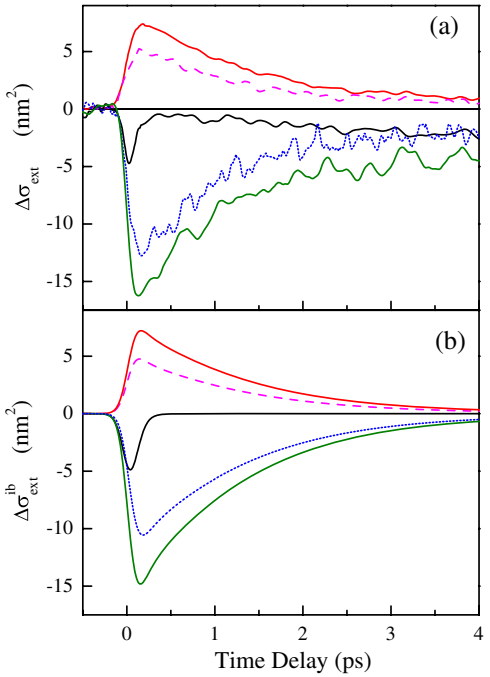


FIG. 2 (color online). (a) Time-dependent $\Delta\sigma_{\text{ext}}(\lambda_{\text{pr}}, t_D)$ measured for the Au nanorod of Fig. 1 at different probe wavelengths $\lambda_{\text{pr}}$ around its SPR: from top to bottom, $\lambda_{\text{pr}} - \lambda_R \approx +30$, $+40$, 0, $-30$, and $-20$ nm ($\lambda_R \approx 810$ nm). (b) Computed interband contribution $\Delta\sigma_{\text{ext}}^{ib}(\lambda_{\text{pr}}, t_D)$ [from Eq. (1)] for the same $\lambda_{\text{pr}}$. The excitation corresponds to $\Delta T_e^{\max} = 125$ K.

silver nanospheres [10]. However, conversely to ensemble measurements, the optical nonlinearity, i.e., $\Delta\epsilon$, underlying the extinction cross-section changes can be quantitatively determined here and the results precisely compared to a theoretical model.

For small changes, $\Delta\sigma_{\rm ext}$ can be straightforwardly connected to the nanorod ultrafast nonlinear response (i.e., the optically induced change of its dielectric function $\epsilon = \epsilon_1 + i\epsilon_2$) by writing it as a linear combination of the changes of $\epsilon_1$ and $\epsilon_2$ induced by the pump pulse:

$$\Delta\sigma_{\rm ext}(\lambda_{\rm pr}, t_D) = a_1(\lambda_{\rm pr})\Delta\epsilon_1(\lambda_{\rm pr}, t_D) + a_2(\lambda_{\rm pr})\Delta\epsilon_2(\lambda_{\rm pr}, t_D) \quad (1)$$

with $a_1 = \partial\sigma_{\rm ext}/\partial\epsilon_1$ and $a_2 = \partial\sigma_{\rm ext}/\partial\epsilon_2$. As the connection between $\sigma_{\rm ext}$ and $\epsilon$ is imposed by the previously determined rod characteristics, i.e., $\eta$ and $V$, $a_1$ and $a_2$ can be computed by using the same finite element method simulations [Fig. 3(a)]. Around the SPR, $a_1$ is almost given by the spectral derivative of the plasmonic resonance: $a_1(\omega) \approx \omega^3/(2\omega_p^2)\partial\sigma_{\rm ext}/\partial\omega$ [Fig. 3(a)]. Its maximum value is thus proportional to $\sigma_{\rm ext}^{\rm max} xQ$, emphasizing that $\Delta\sigma_{\rm ext}$ is proportional to both the amplitude of the SPR and its quality factor $Q$. For short time delays (up to about $t_D \approx 2$ ps), $\Delta\sigma_{\rm ext}$ almost follows the $a_1$ spectral profile [Fig. 3(b)], indicating a dominant $\Delta\epsilon_1$ contribution (yielding a SPR redshift [10,23]). Its normalized induced change can thus be estimated: $\Delta\bar{\epsilon}_1(840\ {\rm nm}, 200\ {\rm fs}) = \Delta\epsilon_1/u_{\rm abs} \approx 2.3 \times 10^{-9}\ {\rm m^3/J}$. For longer time delays, the measured $\Delta\sigma_{\rm ext}$ spectral profile evolves toward the $a_2$ one [Fig. 3(b)]. This indicates an increasing $\Delta\epsilon_2$ contribution (translating into a SPR broadening [10,23]) and yields $\Delta\bar{\epsilon}_2(810\ {\rm nm}, 4\ {\rm ps}) = \Delta\epsilon_2/u_{\rm abs} \approx 1.2 \times 10^{-9}\ {\rm m^3/J}$.

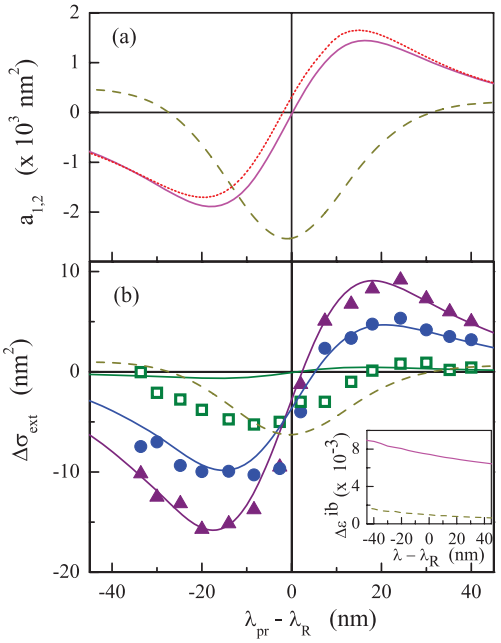


FIG. 3 (color online). (a) Coefficients $a_1$ (solid line) and $a_2$ (dashed line) computed after fitting the $\sigma_{\rm ext}$ spectrum of the nanorod of Fig. 1. The dotted line is calculated from the spectral derivative of $\sigma_{\rm ext}$ (see the text). (b) Ultrafast extinction cross-section changes $\Delta\sigma_{\rm ext}(\lambda_{\rm pr}, t_D)$ around the SPR of the Au nanorod of Fig. 1 measured for three pump-probe delays: $t_D = 0$ fs (dots), 200 fs (triangles), and 4 ps (squares). The electron excitation is $\Delta T_e^{\rm max} = 125$ K. Solid lines: Computed interband contribution $\Delta\sigma_{\rm ext}^{ib}$ for the same time delays. Dashed line: Drude contribution at a long time scale. The inset shows $\Delta\epsilon_1^{ib}$ (solid line) and $\Delta\epsilon_2^{ib}$ (dashed line) computed at $t_D = 200$ fs.

In metal, $\Delta\epsilon_{1,2}(t_D)$ reflect excitation of the electrons by the pump pulse and their subsequent relaxation [22,24]. Fast excitation creates an athermal electron distribution thermalizing internally and with the lattice by electron-electron and electron-phonon scattering, respectively [10]. In bulk metals and not too small particles (larger than about 10 nm), these processes are modeled solving the Boltzmann equation for the electrons, yielding the time- and energy-dependent electron distribution [10,22]. Its modification as compared to the unperturbed one translates into changes of both the interband $\epsilon^{ib}$ (mostly due to $d$-band to conduction-band transitions in gold) and intraband $\epsilon^{Drd}$ (Drude term due to the conduction band electrons) contributions to the metal dielectric function [10,22]: $\Delta\epsilon = \Delta\epsilon^{ib} - \Delta\{\omega_p^2/\omega(\omega + i\gamma)\}$, where $\omega_p$ is the plasma frequency and $\gamma$ the optical scattering rate of the electrons.

On a short time scale, energy is mostly stored in the electrons and $\Delta\epsilon^{ib}$ dominates [22,24]. It can be quantitatively computed from the electronic distribution by using a band structure model, provided the excitation is known (i.e., $u_{\rm abs}$ or $\Delta T_e^{\rm max}$). Conversely to ensemble measurements, this is precisely determined in single particle experiments. The computations show that, away from the interband transition threshold (about 520 nm in gold), $\Delta\epsilon^{ib}$ is weakly dispersed, with a larger $\Delta\epsilon_1^{ib}$ than $\Delta\epsilon_2^{ib}$ amplitude (inset in Fig. 3). By using these values and Eq. (1), the computed time and spectral behaviors of the interband contribution $\Delta\sigma_{\rm ext}^{ib}$ are in good agreement with the experimental ones [Figs. 2(b) and 3(b)]. More precisely, for short time delays, excellent reproductions of both the $\Delta\sigma_{\rm ext}$ dispersion and amplitude are obtained [$t_D = 0$ fs and $t_D = 200$ fs in Fig. 3(b)]. The $\Delta\epsilon_1^{ib}$ contribution dominates for almost all probe wavelengths except around $\lambda_R$, where $a_1$ vanishes, $\Delta\sigma_{\rm ext}$ being then only due to $\Delta\epsilon_2$. The interband term $\Delta\epsilon_2^{ib}$ reflects transient-induced interband absorption at $\lambda_R$ due to reduction of the occupation of the electronic states well below the Fermi energy when the electron distribution is strongly athermal [22]. It is thus nonzero only for a very short time delay, leading to a measured and computed negative transient for $\Delta\sigma_{\rm ext}(\lambda_R)$, almost following the pump-probe correlation [black lines in Figs. 2(a) and 2(b)]. This contribution is also at the origin of the small redshift (as compared to $\lambda_R$) of the

wavelength at which the change of sign of $\Delta\sigma_{\text{ext}}$ takes place [for short time delays; see Fig. 3(b)].

Close to the SPR, $\Delta\epsilon_1^{ib}$ almost follows the total excess energy of the electron distribution [22]. It thus decays with the time constant $\tau_{e\text{-ph}}$, as electron energy is transferred to the lattice and the nanoparticle thermalizes to a temperature close to the initial one (the temperature rising by about 1 K). At a long time scale, the interband contribution becomes negligible [Fig. 2(b)] and does not permit anymore reproduction of the measured $\Delta\sigma_{\text{ext}}$ spectral dispersion and amplitude [Fig. 3(b) for $t_D = 4$ ps]. The residual $\Delta\sigma_{\text{ext}}$ is ascribed to modification of the Drude term due to lattice heating [10,25] and is usually dominated by increase of the electron-phonon scattering rate contribution $\gamma_L$ to $\gamma$. By using the temperature dependence of $\gamma_L$ measured in gold films [26], $\Delta\gamma_L \approx 0.11$ meV is estimated in our experimental conditions. It yields $\Delta\bar{\epsilon}_2^{Drd} \approx 0.8 \times 10^{-9}$ m$^3$/J at the SPR for a thermalized rod, close to the experimental value. Though the computed $\Delta\sigma_{\text{ext}}$ spectral shape is also in agreement with the experimental one [Fig. 3(b)], it is slightly spectrally shifted, indicating additional lattice-mediated contributions (e.g., modification of $\omega_p$ [25]).

The investigated extinction change can also be written in terms of the third-order nonlinear response of the nano-object. Assuming it is much smaller than the wavelength, its optical response close to the SPR corresponds to that of a single dipole: $p(\lambda_{\text{pr}}) = \epsilon_0\epsilon_m\alpha(\lambda_{\text{pr}})E_{\text{pr}}$, oriented along its long axis for a rod [$E_{\text{pr}}$ is the probe optical electric field and $\alpha$ the polarizability of the nanoparticle, its cross section being given by $\sigma_{\text{ext}} \approx \sigma_{\text{abs}} = 2\pi\epsilon_m^{1/2}\,\text{Im}(\alpha)/\lambda_{\text{pr}}$] [27]. Modification of the dipolar response by an ultrafast pump pulse of a duration much smaller than the electron cooling time $\tau_{e\text{-ph}}$ can then be written in terms of a time-dependent nonlinear polarizability, $\alpha = \alpha_L + \alpha_{NL}$, with

$$\alpha_{NL}(\lambda_{\text{pr}}, t_D) = \frac{\partial\alpha_L}{\partial\epsilon_1}\bigg|_{\lambda_{\text{pr}}} \Delta\bar{\epsilon}(\lambda_{\text{pr}}, t_D)\frac{\sigma_{\text{abs}}(\lambda_{pp})}{S_{pp}V}U_{pp}. \quad (2)$$

$U_{pp}$ is the pump-pulse energy, $\lambda_{pp}$ its wavelength, and $\Delta\bar{\epsilon}$ the amplitude of the gold dielectric function change per absorbed energy density, as measured and computed above. Plasmonic effects on the nonlinear response associated to local field enhancement [2] (or to the SPR quality factor $Q$) show up in $\partial\alpha_L/\partial\epsilon_1$ and $\sigma_{\text{abs}}$. The former can be computed numerically by following the method used for $a_1$ and $a_2$. This fully defines the nonlinear polarizability $\alpha_{NL}$ whose time and wavelength dependence can thus be computed (by fully taking into account interband related effects when the SPR overlaps the interband transitions [28]). Similar approaches can be used to predict the nonlinear response of other shape gold nano-objects and straightforwardly extended to other noble metals.

Furthermore, this expression permits one to connect the nonlinear response of a single nano-object to that of an ensemble forming a composite material. For nanorods assumed to be randomly oriented with a small density $n_{np}$ to neglect their interaction, the effective dielectric function of the material is given by orientational averaging of the individual contributions yielding $\epsilon_{\text{eff}} = \tilde{\epsilon}_L + \tilde{\epsilon}_{NL}$, with $\tilde{\epsilon}_L = \epsilon_m(1 + n_{np}\alpha_L/3)$ and $\tilde{\epsilon}_{NL} = \epsilon_m n_{np}\alpha_{NL}/j$. Here $j = 3$ or 5 for polarization-independent or -dependent ($\lambda_{pp} \approx \lambda_R$) pump absorption, respectively. This connection, along with the above theoretical model, can be used to predict the ultrafast nonlinear response of any plasmonic nanostructure and material.

In conclusion, combining the SMS technique with a high sensitivity femtosecond pump-probe experiment, we have quantitatively investigated the ultrafast nonlinear optical response of a single gold nanorod around its SPR. The nonlinear response can be interpreted in terms of the third-order bulk metal nonlinearity enhanced by the plasmonic effect. It is dominated by a Kerr-like nonlinearity due to electron heating, up to a few picoseconds, and by lattice heating after electron-phonon thermalization, in quantitative agreement with a theoretical model. These studies open up many possibilities for investigation and modeling of the optical nonlinearity in plasmonic materials and devices. Extension to other nano-objects or metal or optically nonlinear environments (e.g., a semiconductor) would also be particularly interesting.

The authors acknowledge financial support from CNRS PICS Contract No. 4917. N. D. thanks Institut Universitaire de France.

*delfatti@lasim.univ-lyon1.fr

[1] S. A. Maier, *Plasmonics: Fundamentals and Applications* (Springer, Berlin, 2007).
[2] C. Flytzanis *et al.*, in *Progress in Optics*, Vol. XXIX, edited by E. Wold (North-Holland, Amsterdam, 1991), p. 321.
[3] F. Vallée, in *Nanomaterials and Nanochemistry*, edited by C. Bréchignac, P. Houdy, and M. Lahmani (Springer, Berlin, 2007), p. 197.
[4] J. A. Schuller *et al.*, Nature Mater. **9**, 368 (2010).
[5] K. Willets and R. Van Duyne, Annu. Rev. Phys. Chem. **58**, 267 (2007).
[6] J. Krenn *et al.*, Phys. Rev. Lett. **82**, 2590 (1999).
[7] M. Aeschlimann *et al.*, Nature (London) **446**, 301 (2007).
[8] K. F. MacDonald *et al.*, Nat. Photon. **3**, 55 (2008).
[9] F. Vallée, C. R. Acad. Sci. Paris, Ser. IV **2**, 1469 (2001).
[10] C. Voisin *et al.*, J. Phys. Chem. B **105**, 2264 (2001).
[11] J. J. Mock *et al.*, J. Chem. Phys. **116**, 6755 (2002).
[12] S. Berciaud *et al.*, Nano Lett. **5**, 515 (2005).
[13] H. Baida *et al.*, Nano Lett. **9**, 3463 (2009).
[14] M. Pelton *et al.*, Phys. Rev. B **73**, 155419 (2006).
[15] O. L. Muskens *et al.*, Nano Lett. **6**, 552 (2006).
[16] C. J. Murphy *et al.*, J. Phys. Chem. B **109**, 13 857 (2005).
[17] C. Novo *et al.*, Phys. Chem. Chem. Phys. **8**, 3540 (2006).
[18] O. L. Muskens *et al.*, J. Phys. Chem. C **112**, 8917 (2008).
[19] O. L. Muskens *et al.*, Phys. Rev. B **78**, 205410 (2008).

[20] P. Billaud *et al.*, J. Phys. Chem. C **112**, 978 (2008).
[21] P. B. Johnson and R. W. Christy, Phys. Rev. B **6**, 4370 (1972).
[22] N. Del Fatti *et al.*, Phys. Rev. B **61**, 16 956 (2000).
[23] S. Park *et al.*, J. Phys. Chem. C **111**, 116 (2007).
[24] Y. Guillet, E. Charron, and B. Palpant, Phys. Rev. B **79**, 195432 (2009).
[25] D. T. Owens *et al.*, J. Appl. Phys. **107**, 123114 (2010).
[26] G. R. Parkins, W. E. Lawrence, and R. W. Christy, Phys. Rev. B **23**, 6408 (1981).
[27] C. F. Bohren and D. R. Huffman, *Absorption and Scattering of Light By Small Particles* (Wiley, New York, 1998).
[28] T. V. Shahbazyan, I. E. Perakis, and J. Y. Bigot, Phys. Rev. Lett. **81**, 3120 (1998).